Original Article

Induction of the ER stress response in NRVMs is linked to cardiotoxicity caused by celastrol

Zhong Chen[1,3], Zhong Zhuang[1], Chen Meng[1], Zhonghua Zhu[1], Yin Zhang[1,2,*], and Zhao Zhang[1,*]

[1]Jiangsu Key Laboratory for Molecular and Medical Biotechnology, College of Life Sciences, Nanjing Normal University, Nanjing 210023, China, [2]School of Food Science and Pharmaceutical Engineering, Nanjing Normal University, Nanjing 210023, China, and [3]Jiangsu Key Laboratory of Molecular Medicine of the School of Medicine, Nanjing University, Nanjing 210093, China
*Correspondence address. Tel: +86-25-85891050; E-mail: 2779352842@qq.com (Y.Z.) / E-mail: zhangzhao@njnu.edu.cn (Z.Z.)

Abstract

Celastrol is a quinone methide triterpenoid extracted from the root bark of *Tripterygium wilfordii* Hook F, and it exhibits extensive biological activities such as anti-cancer effects. However, narrow therapeutic window together with undesired side effects limit its clinical application. In this study, we explore celastrol's cardiotoxicity using the methods of histology and cell biology. The results show that celastrol administration dose-dependently induces cardiac dysfunction in mice as manifested by left ventricular dilation, myocardial interstitial fibrosis, and cardio-myocyte hypertrophy. Exposure to celastrol greatly decreases neonatal rat ventricular myocyte (NRVM) viability and promotes its apoptosis. More importantly, we demonstrate that celastrol exerts its pro-apoptotic effects through endoplasmic reticulum (ER) stress and unfolded protein response. Furthermore, siRNA targeting C/EBP homologous protein, a pivotal component of ER stress-mediated apoptosis, effectively prevents the pro-apoptotic effect of celastrol. Taken together, our results demonstrate the potential cardiotoxicity of celastrol and a direct involvement of ER stress in the celastrol-induced apoptosis of NRVMs. Thus, we recommend careful evaluation of celastrol's cardiovascular effects when using it in the clinic.

Key words cardiotoxicity, celastrol, endoplasmic reticulum stress, neonatal rat ventricular myocytes

Introduction

Celastrol, a bioactive compound isolated from *Tripterygium wilfordii* Hook F, has a substantial potential for treating chronic inflammation-related diseases [1–8], including cancers [9–11]. However, its narrow therapeutic window and severe side effects greatly limit its clinical application [12–14]. Sun *et al.* [15] demonstrated that, at 200 nM, celastrol inhibits cardiac Kir2.1 and hERG potassium channels with dual effects on both ion conductivity and protein trafficking, leading to QT prolongation. Recently, Liu and coworkers demonstrated that 2 mg/kg celastrol could induce cardiomyocyte apoptosis and cardiac injury [16]. Considering the wide anti-cancer activities of celastrol, it is necessary to determine celastrol's cardiotoxicity and the potential mechanism involved.

The endoplasmic reticulum (ER) is an organelle playing an essential role in multiple cellular processes, such as protein folding, calcium homeostasis, and lipid biosynthesis [17,18]. Several environmental, physiological, or pathological stimuli, including

toxic compounds, oxidative stress, disordered calcium metabolism, elevated protein synthesis, and nutrients deprivation, can interfere with ER function [19,20], leading to an accumulation of unfolded or misfolded proteins in the ER. This phenomenon is named ER stress. When ER stress occurs, three ER transmembrane sensors are activated, namely, protein kinase R-like ER kinase (PERK), inositol-requiring enzyme 1 (IRE1), and activating transcription factor 6 (ATF6), which initiates an adaptive response called the unfolded protein response (UPR) [20]. Another mechanism that reduces the level of misfolded and unfolded proteins in the ER is degradation via the ER-associated protein degradation (ERAD) pathway [17,18], which retro-translocates these proteins into the cytosol and then degrades them through the ubiquitin–proteasome machinery. If ER stress is prolonged and overwhelmed, ER stress-initiated apoptotic signaling is induced [21]. Interestingly, all of the ER sensor proteins are also responsible for apoptotic signaling, but the factors influencing the cell survival or death remain unclear [22].

Accumulating evidence suggests that ER stress-related signaling pathways are implicated in the pathophysiology of cardiovascular diseases [23,24]. Furthermore, many groups have demonstrated that the UPR and ER stress-initiated apoptosis co-exist in failing hearts and the ER stress-dependent cell death pathway may affect the transition from cardiac hypertrophy to heart failure [25–27]. Notably, increasing evidence shows that ER stress-initiated apoptotic signaling may be involved in the cardiotoxicity of anti-cancer therapy [28–30].

In this study, we investigated the association between ER stress-initiated apoptosis and the cardiotoxicity of celastrol. We examined the effects of celastrol on mouse hearts and investigated the potential mechanism. We demonstrated that celastrol causes cardiac dysfunction in mice and induces neonatal rat ventricular myocyte (NRVM) apoptosis. Moreover, the activation of the ER stress response by celastrol at least partly contributes to its pro-apoptotic effect against cultured cardiomyocytes.

Materials and Methods

Animals and experimental protocols

The animal experiments conformed to the Guide for the Care and Use of Laboratory Animals published by the US National Institutes of Health regulations (NIH publication No. 85-23, revised 148 in 2011). Celastrol powder (L-003; Herbpurify, Chengdu, China) was dissolved it in dimethyl sulfoxide (DMSO) and stored in aliquots at −20°C. Male C57BL/6J mice (8 weeks old; Gempharmatech, Nanjing, China) were randomly assigned into five groups and administered with saline (every day), vehicle (DMSO:PEG300: Tween-80:saline = 1:4:0.5:4.5, every day), or celastrol (1 and 2 mg/kg every day or 4 mg/kg every other day) by intraperitoneal (i.p.) injection. After 2 weeks, the mice were anesthetized using Avertin (250 mg/kg, i.p.) and the two-dimensional guided M-mode and Pulsed-Wave Doppler images were recorded. Each measurement was performed at least in triplicate. The images were analyzed using the VEVO 2100 analysis software (VisualSonics, Toronto, Canada). Animal experiments and echocardiographic measurements were carried out by two independent, blinded operators.

Primary culture of NRVMs

NRVMs were prepared from the ventricles of 1–3-day-old Wistar rats (Gempharmatech) using the method described by Maass *et al.* [31]. Briefly, ventricles collected from the hearts of rat pups were pooled, minced and mixed with 5 mL of pre-warmed trypsin (BD Difco, Michigan, USA) solution (2 mg/mL) as per standard tryptic digestion protocols. After digestion, the supernatants were pooled and centrifuged at 800 g for 5 min. Then, the cells were suspended in Dulbecco's modified Eagle's medium (Invitrogen, Carlsbad, USA) supplemented with 10% fetal bovine serum, penicillin (100 U/mL), and streptomycin (100 μg/mL). Then, cardiomyocytes were purified and cultivated using the differential adhesion method. The cardiomyocyte-enriched media were transferred into another tissue culture dish supplemented with bromodeoxyuridine (100 μM, 19-160; Sigma-Aldrich Chemical, St Louis, USA) to inhibit the proliferation of non-cardiomyocytes for the first 48 h. Finally, the cultured NRVMs were seeded on coverslips or in 24- and 96-well plates for the subsequent assays.

Histological analysis

For histological analysis, the mouse hearts were washed with ice-cold phosphate- buffered saline (PBS) and then fixed in 4% paraformaldehyde overnight. The heart samples were embedded in paraffin and cut longitudinally into 5-μm sections. Serial heart sections were stained with hematoxylin and eosin (HE) or Masson's trichrome for morphology, cellular dimensions, and fibrosis assessment. Digital image analysis was performed blindly with ImageJ software. The cultured NRVMs were incubated with 1.0 μM celastrol for 24 h and then fixed with 95% ethanol for 20 min and stained with HE dye (C0105S; Beyotime Biotechnology, Shanghai, China).

Immunofluorescence analysis

The mouse heart sections were deparaffinized with xylene and then dewatered with ethanol. After heat-induced antigen retrieval, the cell membrane was permeabilized with 0.1% Triton X-100, and non-specific sites were blocked with goat serum (C0265; Beyotime Biotechnology) for 30 min at a room temperature. The sections were then incubated with rabbit polyclonal antibodies against glucose-regulated protein 78 (GRP78) (1:200, GB11098; Servicebio, Wuhan, China) overnight at 4°C, followed by incubation with fluorescein-conjugated secondary antibodies (1:200, A-21428; Invitrogen) for 1 h at a room temperature in the dark. Afterwards, the nuclei were stained with DAPI for 5 min at a room temperature. The images were captured using a fluorescence microscope (Ti-S; Nikon, Tokyo, Japan).

MTT assay

Cell viability was assessed using the MTT cell proliferation and cytotoxicity detection kit (KGA311; KeyGEN Biotech, Nanjing, China). Briefly, NRVMs in a density of 3×10^4 cells/mL were seeded in 96-well plates and exposed to various concentrations of celastrol for 24 h. To inhibit apoptosis, NRVMs were pretreated with the pan-Caspase inhibitor Z-VAD-FMK (10 mM, C1202; Beyotime Biotechnology) for 3 h before treating them with celastrol (1.0 μM for 24 h). Then 50 μL of MTT solution to each well and incubated at 37°C for 4 h. After removal of the medium, 150 μL of DMSO was added to each well to dissolve the formazan crystal. Finally, the absorbance of the dissolved formazan crystal solution was measured at 570 nm using a microplate reader (Thermo Fisher Scientific, Waltham, USA).

Hoechst staining

Cell apoptosis was detected by Hoechst staining. Cultured NRVMs were treated with 1.0 μM or 1.5 μM of celastrol for 24 h. To inhibit the ER stress response, NRVMs were pretreated with 4-PBA (0.5 mM, P21005; Sigma-Aldrich Chemical) for 3 h before treating them with celastrol (1.0 μM for 24 h). Then cells were fixed with 4% paraformaldehyde for 15 min and then stained with Hoechst 33342 dye (1 μg/mL, 14533; Sigma-Aldrich Chemical) for 5 min. After being washed with PBS, cells were mounted on coverslips using glycerol. Then cell images were captured using the fluorescence microscope.

Measurement of mitochondrial membrane potential

Cultured NRVMs were exposed to various concentrations of celastrol for 24 h. Then the mitochondrial membrane potential (ΔΨm) was measured using a mitochondrial membrane potential assay kit (JC-1, C2006; Beyotime Biotechnology) according to the manufacturer's protocol.

Quantitative real-time PCR

Total RNA was extracted from NRVMs using the Trizol reagent (Invitrogen) following the manufacturer's protocol and converted into cDNA using a PrimeScript™ RT reagent (RR047A) kit (TaKaRa, Tokyo, Japan). Quantitative real-time PCR (qRT-PCR) was performed using a SYBR® Premix EXTaq™ (RR420A) kit (TaKaRa) according to the manufacturer's instruction on a StepOnePlus™ Real-Time PCR Detection System (Applied Biosystems, Foster City, USA). The relative mRNA levels were determined by normalizing them to the rat 18s rRNA level. The qPCR conditions were: 95°C for 30 s, followed by 40 cycles at 95°C for 5 s, 60°C for 34 s. Detailed primer sequences are presented in Table 1. XBP1 splicing was detected using the following primers: forward 5′-ACGAGAGAAAACTCATGG-3′ and reverse 5′-ACAGGGTCCAACTTGTCC-3′. These primer pairs could detect both unspliced XBP1 (290 bp) and spliced XBP1 (264 bp).

Caspase-3 activity assay

Cultured NRVMs were seeded into 6-well plates and incubated with various concentrations of celastrol for 24 h. Caspase-3 activity was assessed using a Caspase-3 colorimetric assay kit (KGA204; KeyGEN Biotech) according to the manufacturer's protocol.

Western blot analysis

NRVMs were washed with cold PBS and lysed with 1 × SDS-PAGE sample buffer (45 mM Tris-HCl, pH 6.8, 10% glycerol, 1% SDS, 0.01% bromophenol blue, and 0.05 mM DTT) supplemented with 1 mM PMSF and a protease inhibitor cocktail (Roche, Mannheim, Germany). The lysates were boiled at 99°C for 10 min, separated by 12% SDS-PAGE, and then transferred onto PVDF membranes. The PVDF membranes were blocked with 5% non-fat milk in Tris-buffered saline containing 0.1% Tween-20 (TBST) for 1 h at a room temperature, followed by overnight incubation at 4°C with the appropriate primary antibodies against C/EBP homologous protein (CHOP) (1:500, sc-7351; Santa Cruz Biotechnology, Dallas, USA), ubiquitin (1:500, sc-8017; Santa Cruz Biotechnology), GRP78 (1:500, BS6479; Bioworld Technology, Shanghai, China), eukaryotic initiation factor 2α (eIF2α) (1:500, BS3651; Bioworld Technology), and phosphorylated eIF2α at Ser51 (p-eIF2α) (1:500, BS4787; Bioworld Technology). The membranes were washed with TBST and incubated with HRP-conjugated secondary antibodies (1:10,000, BS13278, BS12478; Bioworld Technology). Finally, the protein blots were visualized using an enhanced chemiluminescence kit (Bio-Rad, Hercules, USA) with the Fluor Chem E System (Cell Biosciences, Santa Clara, USA). To promote ER stress in NRVMs, we used thapsigargin (1.0 μM, T9033; Sigma-Aldrich Chemical) as a positive control.

Immunofluorescence microscopy

Cultured NRVMs were seeded on coverslips. After treatment with 1.0 μM celastrol for 12 h, the cells were fixed in 4% paraformaldehyde for 15 min, permeabilized with 0.1% Triton X-100 for 30 min, and then blocked in 3% BSA for 30 min at a room temperature. Then, cells were incubated with mouse monoclonal antibodies against calnexin (1:100, ab112995; Abcam, Cambridge, UK) at 37°C for 2 h, followed by incubation with Alexa Fluor 555-conjugated goat anti-mouse IgG (H + L) (1:200, A-21422; Invitrogen) at 37°C for

2 h. After wash with PBST (0.1% Tween-20 in PBS), cells were stained with Hoechst 33342 (1 μg/mL) for 5 min at a room temperature Finally, cells were washed with PBST and cell images were capture with a confocal microscope (A1; Nikon, Tokyo, Japan).

Transfection of small interfering RNA

Cultured NRVMs were seeded in 6-well plates and transfected with siCHOP using Lipofectamine 3000 (Invitrogen) according to the manufacturer's instructions. The rat CHOP-specific small interfering RNA (siRNA) and scrambled control siRNA were purchased from Invitrogen. The sequences are as follows: siCHOP, 5′-CGAAGAGGAAGAAUCAAA-3′; scramble control siRNA, 5′-UU-CUCCGAACGUGUCACGUTT-3′. The effectiveness of siCHOP in different concentrations was confirmed by western blot analysis. After transfection, cells were treated with 1.0 μM celastrol for 24 h and collected for subsequent analysis.

Statistical analysis

Data are presented as the mean ± standard deviation (SD) from at least three independent experiments. Pairs of groups were compared using Student's two-tailed t-test and multiple groups were compared using one-way ANOVA with Tukey's HSD post hoc. All statistical analyses were performed using SPSS 21.0 software. $P < 0.05$ was considered statistically significant.

Results

Celastrol causes cardiac dysfunction and myocardial fibrosis in mice

Mice were injected with three different doses of celastrol following the administration regimen. To explore the potential effects of celastrol on mice, we first monitored the mice's bodyweight. Figure 1A shows that celastrol remarkably decreased the bodyweight of exposed mice compared with the controls, implying that celastrol suppresses food intake or enhances energy expenditure, leading to weight loss. Next, echocardiographic measurements were performed to determine the cardiotoxic effects of celastrol. As shown in Figure 1B,C, treatment with a low dose of celastrol (1 mg/kg/day) for 2 weeks had no significant effect on the heart weight, cardiac contractile function, or heart structure. However, treatment with a medium dose (2 mg/kg/day) or a high-dose (4 mg/kg every 2 days)

Table 1. Sequences of primers used in RT-qPCR

| Gene	Forward primer (5′→3′)	Reverse primer (5′→3′)
Bcl-2	CGACTTTGCAGAGATGTCCA	ATGCCGGTTCAGGTACTCAG
Bax	TGCAGAGGATGATTGCTGAC	GATCAGCTCGGGCACTTTAG
Caspase-3	AATTCAAGGGACGGGTCATG	GCTTGTGCGCGTACAGTTTC
Caspse-12	CTCTTCATTTCCAAACTCGTTGACT	GGGCATCTGGGTCAGTTCAC
GRP78	AACCCAGATGAGGCTGTAGCA	ACATCAAGCAGAACCAGGTCAC
CHOP	TGGCACAGCTTGCTGAAGAG	TCAGGCGCTCGATTTCCT
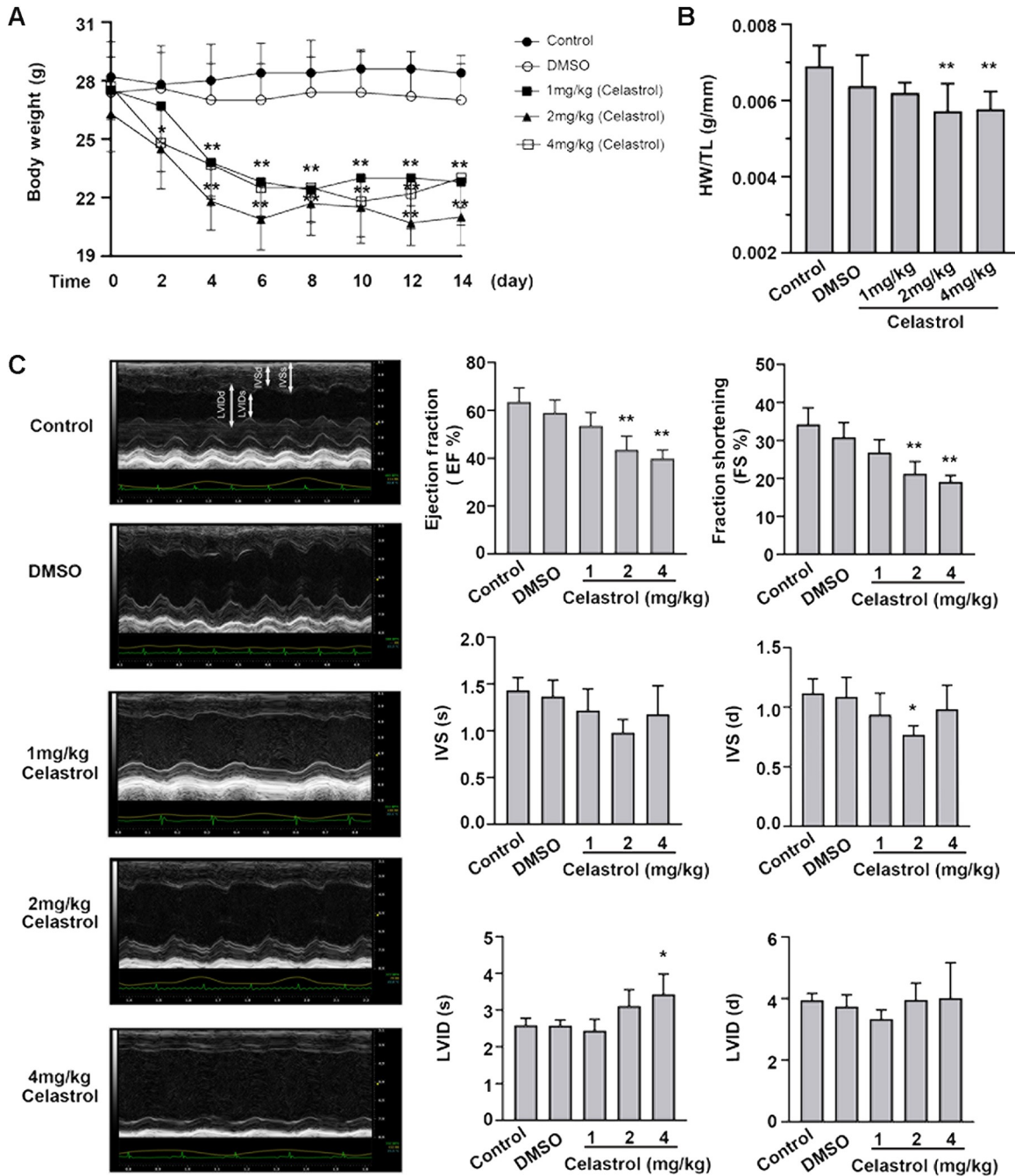
Figure 1. Celastrol impairs cardiac function in mice (A) Mice bodyweight in each group, recorded at 1-day intervals ($n = 10$ mice per group). (B) The heart weight to tibia length ratio (HW/TL) in each group ($n = 10$ mice per group). (C) Representative echocardiographic images of the left ventricles from the five groups, echocardiographic parameters (left ventricular ejection fraction (EF%), left ventricular fractional shortening (FS%), end-systolic and end-diastolic interventricular septum thickness (IVSs and IVSd), and end-systolic and end-diastolic dimension of the left ventricle (LVIDs and LVIDd)) presented as the mean ± SD in bar graphs illustrating the impaired contractility of the celastrol-treated mice ($n = 10$ mice per group). One-way ANOVA with Tukey's HSD post hoc was used to test the statistical significance. $*P < 0.05$ and $**P < 0.01$ vs controls.

of celastrol for 2 weeks caused a notable decline of heart weight and contractile function, along with cardiac structural remodeling relative to the controls, as indicated by the reduced heart weight to tibia length ratio (HW/TL), ejection fraction (EF%), fraction shortening (FS%), and end-diastolic interventricular septum thickness (IVSd) as well as the increased end-systolic dimension of the left ventricle (LVIDs).

Furthermore, the histological analysis revealed that medium and high doses of celastrol significantly increased the cross-sectional areas of cardiomyocytes (Figure 2A,B) and fibrosis in the interstitial spaces (Figure 2A,C) relative to the controls, further demonstrating that celastrol dose-dependently induces myocardial injury and
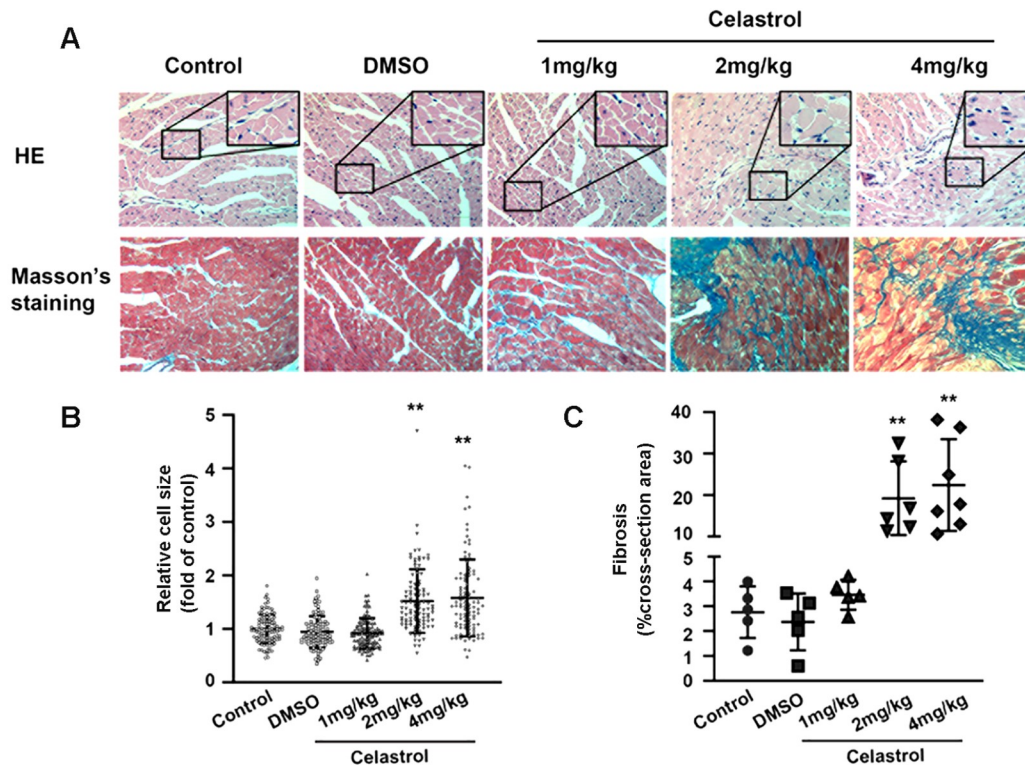
Figure 2. Celastrol causes cardiomyocyte hypertrophy and cardiac interstitial fibrosis in mice (A) Representative HE (*top*) and Masson's trichrome (*bottom*) staining images of the left ventricular sections from the five groups. Scale bar: 50 μm. (B) Statistical comparison of the cross-sectional area of cardiomyocytes in different groups ($n = 100$ cells from three hearts per group, *left*). Each cell size in the indicated group relative to the control group is presented on the scatter plots. Statistical comparison of the fibrotic areas in different groups ($n = 5$–7 fields from three hearts per group, *right*). The fibrotic area quantification relative to the section areas is presented on the scatter plots. One-way ANOVA with Tukey's HSD post hoc was used to test the statistical significance. $**P < 0.01$ vs controls.

cardiac dysfunction. Moreover, mice in the medium- and high-dose groups displayed some side effects on other tissues, including kidney weight reduction and hepatotoxicity (weight loss and inflammatory cell infiltration) (Supplementary Figure S1). Collectively, these results suggest that celastrol is dose-dependently cardiotoxic and induces pathological cardiac remodeling.

Celastrol reduces cell viability and promotes apoptosis in NRVMs

To investigate the *in vitro* cytotoxicity of celastrol, we assessed the viability of primary rat cardiomyocytes in response to celastrol by MTT assays. As shown in Figure 3A, celastrol concentration-dependently inhibited NRVM viability. From 1.0 μM, celastrol significantly decreased NRVM viability. Consistently, the microscopic images indicated that celastrol dose-dependently increased the number of drifting cells and reduced the rate of cell attachment (Figure 3B). Notably, the HE-staining images of NRVMs clearly showed that cytoplasmic vacuoles appeared after exposure to 1.0 μM celastrol for 24 h (Figure 3C). The Hoechst 33342-staining images demonstrated that celastrol effectively induced apoptosis in NRVMs as indicated by the condensed and fragmented nuclei. Moreover, at 1.0 μM and 1.5 μM, celastrol significantly increased the percentage of apoptotic cardiomyocytes (Figure 3D). We also observed necrosis in NRVMs treated with celastrol (1.0 or 1.5 μM, for 24 h), but it contributed far less to cell death than apoptosis did (Supplementary Figure S2).

To further characterize celastrol-induced apoptosis, we detected mitochondrial ΔΨm in NRVMs using the JC-1 fluorescent probe. Treatment with 1.0 μM celastrol for 12 h disrupted the mitochondrial ΔΨm, as evidenced by the markedly increased green fluorescence intensity (Supplementary Figure S3). The JC-1 staining images revealed that 24 h of celastrol treatment decreased the red/green fluorescence intensity ratio by almost 50% compared with the control group (Figure 4A). Moreover, we explored how celastrol affects apoptosis-related genes. Celastrol (1.0 μM for 12 h) down-regulated Bcl-2 expression and up-regulated Bax, Caspase-3, and Caspase-12 mRNA levels in NRVMs compared with the control group (Figure 4B,C). Meanwhile, the activity of Caspase-3, which plays a crucial role in apoptosis, was increased in NRVMs treated with increasing concentrations of celastrol for 24 h (Figure 4D). These results confirm that the apoptotic pathway plays a role in celastrol-mediated cardiomyocyte death. To inhibit apoptosis, we pretreated NRVMs with the pan-Caspase inhibitor Z-VAD-FMK (10 mM) for 3 h before treating them with celastrol (1.0 μM for 24 h). This Z-VAD-FMK pretreatment significantly increased cell viability compared with celastrol treatment alone (Figure 4E). Overall, these results suggest that celastrol-induced apoptosis substantially contributes to celastrol cytotoxicity.

Celastrol induces ER stress and activates the UPR pathway

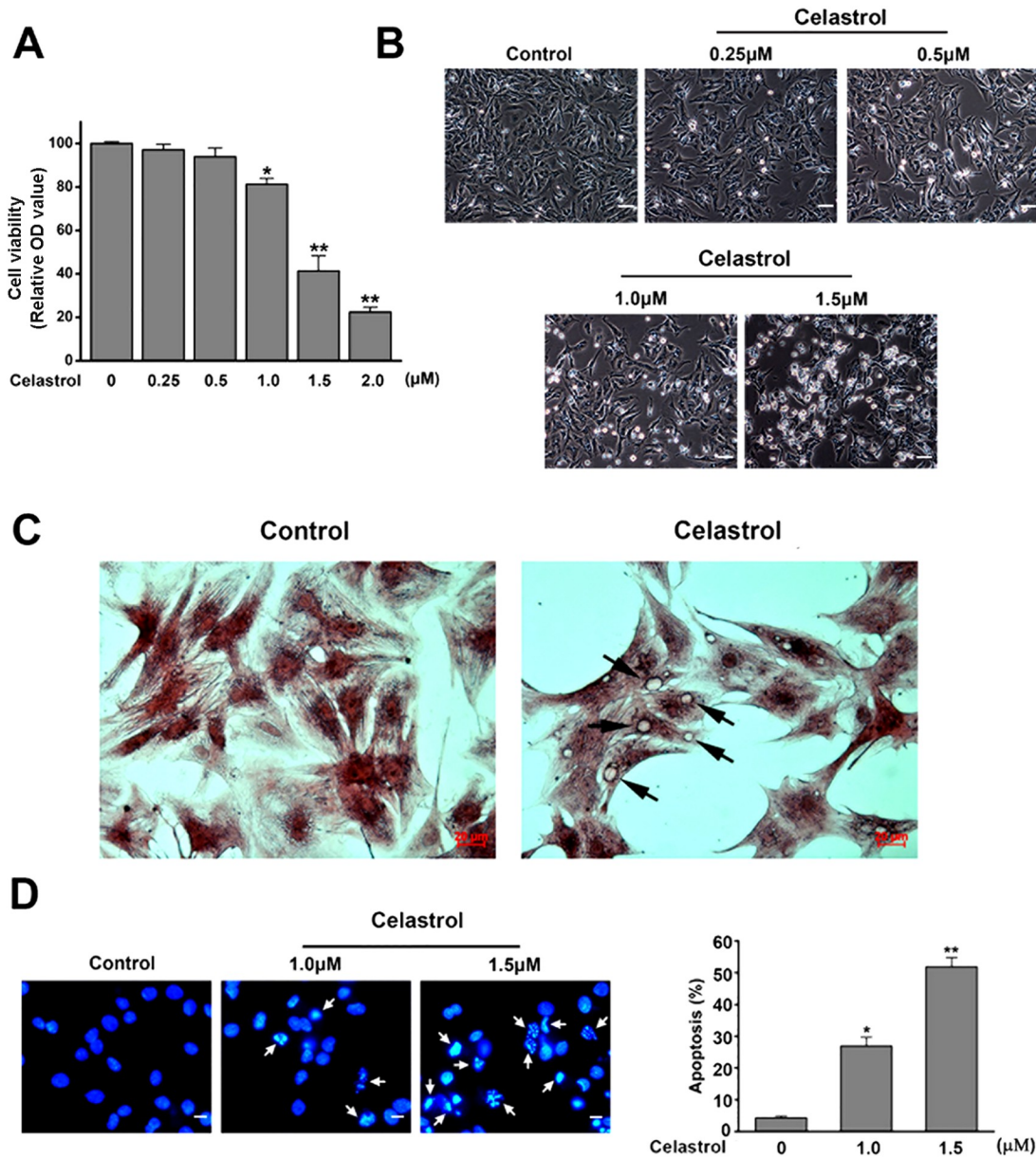Celastrol is a natural proteasome inhibitor [9]. To confirm that

Figure 3. Celastrol attenuates cell viability and induces cytoplasmic vacuoles in NRVMs (A) Results of the cell viability MTT assay ($n = 3$ per group). The cultured NRVMs were incubated with increasing concentrations of celastrol for 24 h. (B) Light micrograph images of NRVMs treated with or without celastrol. Scale bar: 100 μm. Cells were treated with 0.25, 0.5, 1.0, and 1.5 μM celastrol for 24 h. (C) Representative HE-staining images of NRVMs treated with or without 1.0 μM celastrol for 24 h. Scale bar: 20 μm. The black arrows indicate cytosolic vacuoles observed in the celastrol-treated NRVMs. D. Representative Hoechst 33342-staining images of the nucleus morphology of NRVMs treated with celastrol. Scale bar: 20 μm. Cells were treated with 1.0 μM or 1.5 μM of celastrol for 24 h. The white arrows indicate the condensed or fragmented nuclei observed in the celastrol-treated cells (*left*). Quantitative analysis results of the ratio of apoptotic cells treated with or without celastrol treatment ($n = 6$ per group, *right*). One-way ANOVA with Tukey's HSD post hoc was used to test the statistical significance. $*P < 0.05$ and $**P < 0.01$ vs controls.

celatrol inhibits the proteasome in cultured NRVMs, we performed an immunoblot assay and analyzed protein ubiquitination in whole-cell lysates. Treatment of NRVMs with various doses of celastrol for

2 h markedly increased the ubiquitinated proteins levels. Notably, the accumulation of ubiquitinated proteins occurred as early as 1 h after the addition of 1.0 μM celastrol (Figure 5A), much earlier than the mitochondrial ΔΨm disruption. We also checked the ER morphology in NRVMs by staining the ER membrane protein

calnexin. As shown in Figure 5B, vacuoles appeared in cells treated with 1.0 μM celastrol for 12 h. These data indicate that considerable celastrol-induced proteasome inhibition is the early event that may trigger ER stress and the UPR pathway in NRVMs.

To test this hypothesis, we first analyzed the expressions of ER stress-related genes in response to celastrol. The results showed that celastrol-treated NRVMs (0.5, 0.75 and 1.0 μM for 12 h) had significantly elevated levels of GRP78 (Figure 6A,B), an ER stress marker released to assist the folding of accumulated proteins.
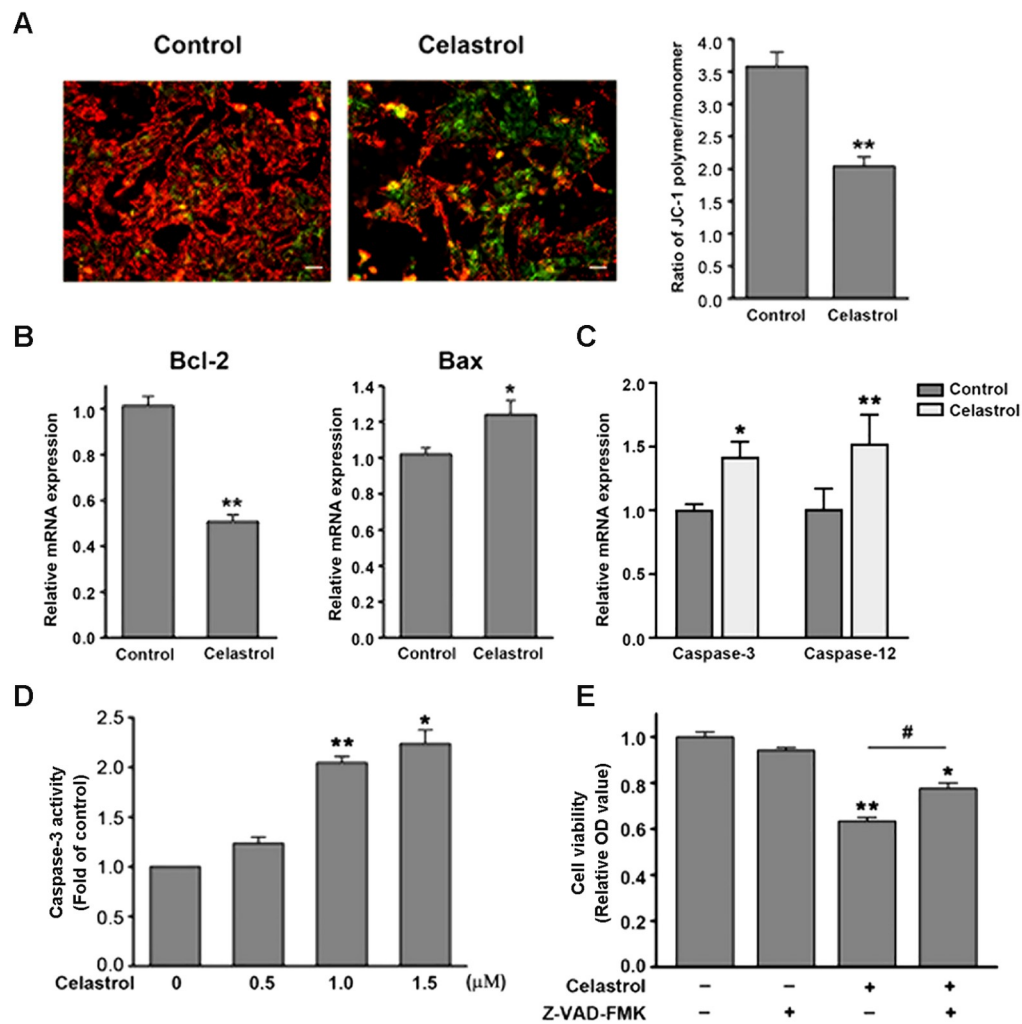
Figure 4. Celastrol induces apoptosis in NRVMs (A) Representative JC-1 staining images of the NRVMs treated with or without 1.0 μM of celastrol for 24 h. Scale bar: 20 μm. JC-1 exhibited potential-dependent accumulation in the mitochondria, indicated by the fluorescence emission shift from green (JC-1 monomers) to orange-red (JC-1 polymers). The increased green to orange-red fluorescence ratio indicates a decrease in the mitochondrial ΔΨm of the NRVMs treated with celastrol (*left*). Quantitative analysis result of the ratio of JC-1 polymers/monomers in the NRVMs treated with or without 1.0 μM of celastrol for 24 h ($n = 4$ per group, *right*). (B) The mRNA levels of genes involved in apoptosis, *Bcl-2* (*left*) and *Bax* (*right*) in the celastrol-treated NRVMs relative to those in the controls ($n = 4$ per group). (C) The mRNA levels of Capase-3 and Caspase-12 in the celastrol-treated NRVMs relative to those in the controls ($n = 4$ per group). (D) The Caspase-3 activity of the celastrol-treated NRVMs relative to the controls ($n = 3$ per group). E. Results of the cell viability MTT assay ($n = 3$ per group). Cultured NRVMs were incubated with celastrol (1.0 μM for 24 h) with or without 3 h of pretreatment with 10 mM Z-VAD-FMK, an inhibitor of apoptosis. Student's two-tailed *t*-test was used to test the statistical significance. *$P < 0.05$ and **$P < 0.01$ vs controls; #$P < 0.05$ vs celastrol treatment without Z-VAD-FMK.

Consistent with the *in vitro* results, celastrol dose-dependently induced the GRP78 expression in the mouse hearts (Supplementary Figure S4). Meanwhile, the protein expression of CHOP was notably up-regulated as early as 6 h after treatment with 1.0 μM celastrol (Figure 6C). This up-regulation was dose-dependent (Figure 6D). Furthermore, we examined the expressions of UPR-related genes. The UPR is characterized by the action of three signaling proteins: ATF6, PERK, and IRE1. Our results revealed that celastrol increased the ATF6 mRNA level in time- and dose-dependent manners. As shown in Figure 6E, cells treated with 1.0 μM of celastrol had markedly increased PERK-regulated phosphorylation of eIF2α (p-eIF2α) after 30 min of treatment. Additionally, celastrol time- and dose-dependently induced the IRE1-mediated cleavage of the XBP1 mRNA precursor (unspliced XBP1) into mature XBP1 mRNA

(spliced XBP1) (Figure 6F). Taken together, our results indicate that celastrol induces proteasome-inhibition-dependent ER stress and activates the resultant UPR pathway in NRVMs, which might be the primary mechanism of celastrol-induced cytotoxicity.

Celastrol causes CHOP-dependent ER stress-induced apoptosis

To confirm whether celastrol induces cardiomyocyte apoptosis through the ER stress-mediated apoptotic pathway, we analyzed the apoptotic cell population and the expressions of related genes in the presence of 4-PBA (0.5 mM). Celastrol (1.0 μM) induced primary cardiomyocyte apoptosis, and pretreatment of cells with 4-PBA for 3 h abrogated this effect (Figure 7A). Furthermore, 4-PBA prevented the celastrol-induced decrease of Bcl-2 level and increase of Bax
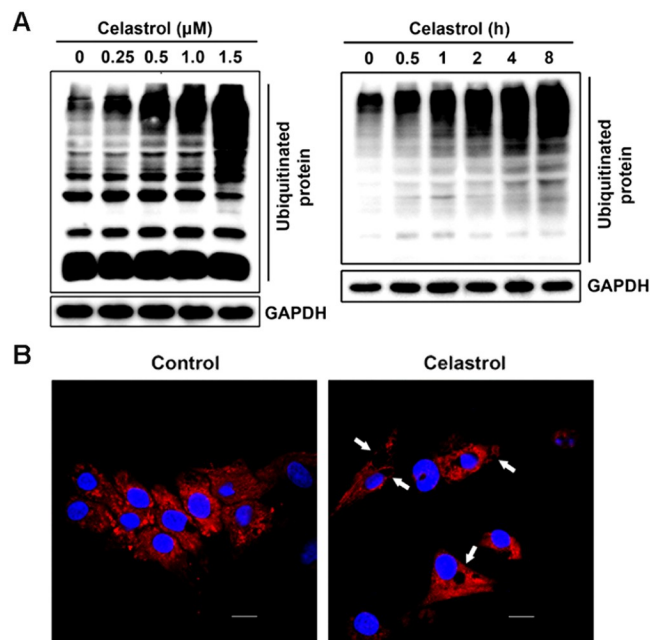
Figure 5. Celastrol increases the accumulation of ubiquitinated proteins in NRVMs (A) Representative immunoblot images of ubiquitinated proteins in the NRVMs after exposure to various concentrations of celastrol for 24 h (*left*) or to 1.0 μM celastrol at indicated time points (*right*). (B) Representative confocal images of the NRVMs treated with or without 1.0 μM of celastrol for 12 h. Scale bar: 10 μm. The ER was localized by staining calnexin (an ER membrane protein), and the cell nucleus was stained with Hoechst 33342. The white arrows indicate the cytosolic vacuoles observed in the celastrol-treated cells using calnexin staining.

expression and Caspase-3 activity (Figure 7B,C). Moreover, 4-PBA pretreatment markedly attenuated the celastrol-induced changes in ER stress-related gene expressions (*GRP78* and *ATF6*) (Figure 7D). The CHOP-dependent pathway is the most common ER stress-mediated apoptotic mechanism [32,33]. In line with these findings, our results showed that 4-PBA notably down-regulated CHOP expression in NRVMs exposed to 1.0 μM of celastrol for 24 h (Figure 7E). To further identify the role of CHOP in celastrol-induced apoptosis in NRVMs, we next blocked the CHOP pathway with CHOP siRNA. CHOP siRNA effectively decreased CHOP expression in celastrol-treated NRVMs (Figure 7F). Figure 7G shows the representative morphological changes in nuclei labeled by Hoechst 33342 under different treatments. Knockdown of *CHOP* significantly reduced the pro-apoptotic effects of celastrol (Figure 7H) and improved cell viability (Figure 7I). These findings confirm that ER stress activation mediates the pro-apoptotic effects of celastrol in NRVMs, which is mediated at least partly by the CHOP-dependent pathway.

Discussion

Celastrol, a robust bioactive compound derived from the *Tripterygium wilfordii* Hook F, used in traditional Chinese medicine, has attracted interest due to its multiple promising biological activities [34,35]. Accumulating evidence has demonstrated that celastrol exhibits anti-cancer activity against many human tumor cell lines and animal cancer models [36–45]. However, celastrol's narrow therapeutic window is a great concern regarding its clinical application. In general, low concentrations are inefficient, and high concentrations show signs of toxicity.

In the present study, we investigated the pharmacological action of celastrol on the heart, using three doses commonly used in various tumor xenograft models [9,10,46–50]. Our results showed

that celastrol-treated mice exhibited notable cardiomyocyte enlargement, fibrosis, and systolic dysfunction. Furthermore, the *in vitro* experiments revealed that celastrol induced apoptosis and reduced cell viability in primary cardiomyocytes. Mechanistically, a perturbation in the ubiquitin-proteasome system and the consequent ER stress response may play a crucial part in celastrol-induced cardiotoxicity. Celastrol is a very effective suppression agent against tumor cells, however, its cardiotoxicity is a major concern for patients with cancer. Thus, celastrol use should be very careful.

Celastrol is a quinone methide triterpenoid capable of reacting with the nucleophilic thiol groups of cysteine residues in proteins [51]. Yang *et al.* [9] first reported that celastrol could directly target the proteasome. Using cell-free proteasome activity assays and computational methods, different groups have demonstrated that celastrol inhibits the chymotrypsin-like activity of the 20S proteasome, leading to the accumulation of ubiquitinated proteins [10,52–54]. Consistent with these reports, we found that, in cultured primary cardiomyocytes, the levels of ubiquitinated proteins were increased as early as 1 h after celastrol addition and did so in concentration and time-dependent manners. The ubiquitin/proteasome-mediated pathway is essential for protein homeostasis maintenance. Proteasomal activity inhibition causes many endogenous proteins, including misfolded or damaged proteins, to accumulate, which induces ER stress, and finally apoptosis [55–58]. A number of studies have demonstrated that celastrol could induce ER stress via inhibition of proteasome activity, leading to apoptosis in different kinds of cancer cells [52,11]. Some group also identified that celastrol induced ER stress-mediated cell apoptosis and inhibited tumor growth in hepatoma H22-bearing mice [54]. Our results revealed that celastrol-treated cultured primary cardiomyocytes displayed increased levels of UPR-related genes (*GRP78* and
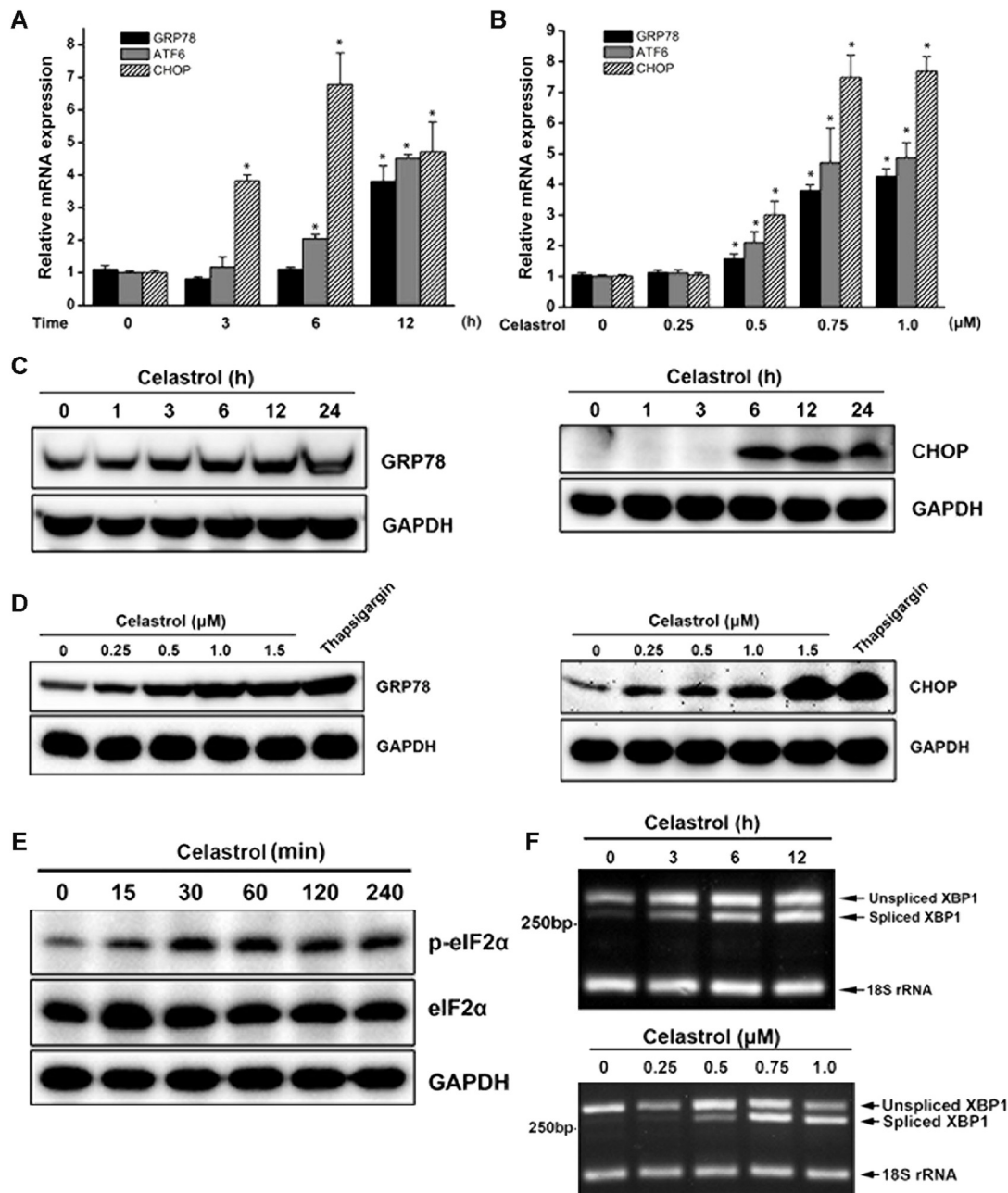
Figure 6. Celastrol induces ER stress in NRVMs (A) The mRNA levels of the ER stress-related genes *GRP78, ATF6*, and *CHOP* in NRVMs treated with 1.0 μM of celastrol for 3, 6, or 12 h relative to those in the controls (*n* = 4 per group). (B) The mRNA levels of the ER stress-related genes *GRP78, ATF6*, and *CHOP* in NRVMs treated with various concentrations of celastrol for 12 h relative to those in the controls (*n* = 4 per group). (C) Immunoblot showing the changes in GRP78 (*left*) and CHOP (*right*) expression in NRVMs treated with 1.0 μM celastrol at indicated time points. (D) Immunoblot showing the changes in GRP78 (*left*) and CHOP (*right*) expression in NRVMs treated with various celastrol concentrations for 24 h. (E) Immunoblot showing the phosphorylation level of eIF2α in NRVMs treated with 1.0 μM of celastrol at indicated time points. (F) Representative agarose electrophoresis image of XBP1 mRNA (*left*). The XBP1 spliced mRNA level in NRVMs treated with various concentrations of celastrol for 12 h (*right*). Positive control: 1.0 μM thapsigargin. One-way ANOVA with Tukey's HSD post hoc was used to test the statistical significance. *$P < 0.05$ and **$P < 0.01$ vs controls.

ATF6), eIF2α phosphorylation and XBP1 splicing, confirming that celastrol can induce ER stress and activate all three branches of the UPR. In agreement with this concept, the *in vivo* experiment also demonstrated the induction of ER stress in the celastrol-treated mouse hearts, as evidenced by increased expression of the UPR chaperone GRP78.

Many lines of evidence demonstrate that ER stress and the resultant UPR signaling pathway play a crucial role in the development of cardiac diseases [22,23]. Clinical evidence and *in vivo* studies have shown that UPR activation and ER stress-initiated apoptotic signaling are associated with the pathophysiology of cardiac hypertrophy and heart failure [25,26]. Proteins such as
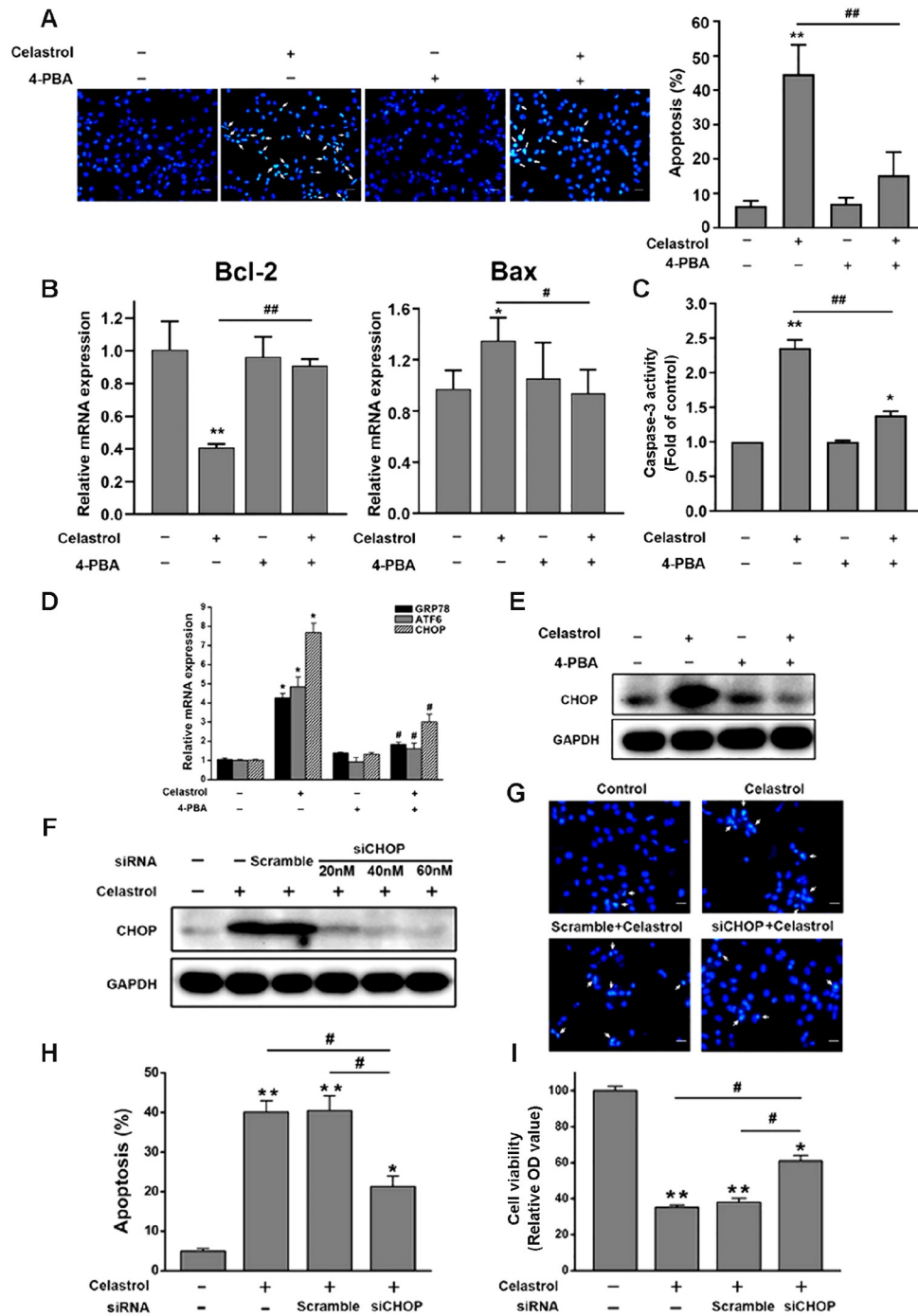
Figure 7. Blocking the ER stress signaling pathway prevents celastrol-induced apoptosis in NRVMs (A) Representative Hoechst 33342-staining images showing the nucleus morphology of NRVMs pretreated with 0.5 mM 4-PBA for 3 h before celastrol treatment (1.0 μM for 24 h). Scale bar: 50 μm. The white arrows indicate the condensed or fragmented nuclei observed in the celastrol-treated cells. Quantitative analysis of the apoptotic cells ratio ($n = 6$ per group). (B) The *Bcl-2* and *Bax* mRNA levels in NRVMs pretreated with 4-PBA (0.5 mM) for 3 h before exposure to 1.0 μM celastrol for 12 h. (C) The Caspase-3 activity of the celastrol-treated NRVMs pretreated with 4-PBA (0.5 mM) for 3 h. (D) The *GRP78*, *ATP6*, and *CHOP* mRNA levels in NRVMs pretreated with 0.5 mM 4-PBA for 3 h before exposure to 1.0 μM celastrol for 12 h. (E) Immunoblot image of CHOP in celastrol-treated NRVMs before treatment with 4-PBA. (F) Immunoblot showing the changes in CHOP expression in the NRVMs. The cells were transfected with various siCHOP for 24 h, and then treated with 1.0 μM of celastrol for 24 h. (G) Representative Hoechst 33342-staining images showing the nucleus morphology of NRVMs treated with or without celastrol after transfection. Scale bar: 50 μm. The white arrows indicate the condensed or fragmented nuclei observed in celastrol-treated cells. (H) Quantitative analysis of the apoptotic cells ratio ($n = 6$ per group). (I) Results of the cell viability MTT assay ($n = 3$ per group). Cultured NRVMs were incubated with or without 1.0 μM celastrol for 24 h after transfection. Student's two-tailed *t*-test was used to test the statistical significance. *$P < 0.05$ and **$P < 0.01$ vs controls; #$P < 0.05$ and ##$P < 0.01$ vs the celastrol without 4-PBA group or the celastrol with scramble group.

Caspase-12, c-JUN NH2-terminal kinase, and CHOP participate in the ER stress-initiated apoptotic signaling pathway [21]. Several studies suggested that the CHOP-dependent cell death pathway participates in the transition from cardiac hypertrophy to heart failure [27,59]. CHOP is the most common ER stress-mediated apoptotic protein [32,33,60], and it is mainly regulated by PERK/eIF2α- and ATF6-dependent pathways [17,18]. CHOP decreases the anti-apoptotic factor/pro-apoptotic factor ratio (Bcl-2/Bax), leading to cell apoptosis [59,61]. Hu et al. [62] showed that proteasome inhibition induces ER stress-initiated cardiomyocyte death via a CHOP-dependent pathway. In the present study, we found that celastrol-treated cardiomyocytes had significantly increased CHOP mRNA level after the activation of the ATF6- and PERK/eIF2α-dependent pathways.

Moreover, UPR activation and the sequential up-regulation of CHOP expression occurred much earlier than mitochondrial Δψm disruption, suggesting that ER stress is an early event that initiates the intrinsic apoptosis. CHOP also stimulates calcium release by the ER, which could provoke mitochondria-dependent apoptosis through the release of mitochondrial cytochrome c and loss of mitochondrial membrane potential [63,64]. However, further investigation on the correlation between mitochondrial dysfunction and ER stress in the celastrol-treated cardiomyocytes could provide a better understanding of the celastrol-induced apoptotic effects. Moreover, treatment of cells with CHOP siRNA considerably inhibited cardiac apoptosis, suggesting that CHOP is important for the celastrol-induced pro-apoptotic signaling. Many studies have demonstrated that anti-cancer drugs, such as bortezomib, imatinib and doxorubicin, can directly induce ER stress-initiated apoptotic signaling, thus contributing to the cardiovascular complications they induced [28–30]. Based on these findings, we recommend that the cardiotoxicity of celastrol should be taken into account when using it in anti-cancer therapy.

In summary, we showed that celastrol could trigger ER stress-initiated apoptosis in cardiomyocytes. Although elucidating the complicated mechanism of celastrol-mediated cardiotoxicity requires more research, our findings suggest that its clinic use needs special attention. Further trials, such as combination therapy, structural celastrol derivatives, and nano/micro-systems development, may help to improve the rational use of celastrol in clinic,

Supplementary Data
Supplementary data is available at *Acta Biochimica et Biophysica Sinica* online.

Funding

Conflict of Interest
The authors declare that they have no conflict of interest.

References

1. Tao X, Younger J, Fan FZ, Wang B, Lipsky PE. Benefit of an extract ofTripterygium Wilfordii Hook F in patients with rheumatoid arthritis: A double-blind, placebo-controlled study. *Arthritis Rheum* 2002, 46: 1735–1743

2. Allison AC, Cacabelos R, Lombardi VRM, Álvarez XA, Vigo C. Celastrol, a potent antioxidant and anti-inflammatory drug, as a possible treatment for Alzheimer's disease. *Prog Neuropsychopharmacol Biol Psychiatry* 2001, 25: 1341–1357

3. Paris D, Ganey NJ, Laporte V, Patel NS, Beaulieu-Abdelahad D, Bachmeier C, March A, *et al.* Reduction of β-amyloid pathology by celastrol in a transgenic mouse model of Alzheimer's disease. *J Neuroinflammation* 2010, 7: 17

4. Liu J, Lee J, Salazar Hernandez MA, Mazitschek R, Ozcan U. Treatment of obesity with celastrol. *Cell* 2015, 161: 999–1011

5. Ma X, Xu L, Alberobello AT, Gavrilova O, Bagattin A, Skarulis M, Liu J, *et al.* Celastrol protects against obesity and metabolic dysfunction through activation of a HSF1-PGC1α transcriptional axis. *Cell Metab* 2015, 22: 695–708

6. Li H, Zhang YY, Tan HW, Jia YF, Li D. Therapeutic effect of tripterine on adjuvant arthritis in rats. *J Ethnopharmacol* 2008, 118: 479–484

7. Morita T. Celastrol: a new therapeutic potential of traditional Chinese medicine. *Am J Hypertension* 2010, 23: 821

8. Pinna GF, Fiorucci M, Reimund JM, Taquet N, Arondel Y, Muller CD. Celastrol inhibits pro-inflammatory cytokine secretion in Crohn's disease biopsies. *Biochem Biophys Res Commun* 2004, 322: 778–786

9. Yang H, Chen D, Cui QC, Yuan X, Dou QP. Celastrol, a triterpene extracted from the Chinese "Thunder of God Vine," is a potent proteasome inhibitor and suppresses human prostate cancer growth in nude mice. *Cancer Res* 2006, 66: 4758–4765

10. Ge P, Ji X, Ding Y, Wang X, Fu S, Meng F, Jin X, *et al.* Celastrol causes apoptosis and cell cycle arrest in rat glioma cells. *Neurol Res* 2010, 32: 94–100

11. Fribley AM, Miller JR, Brownell AL, Garshott DM, Zeng Q, Reist TE, Narula N, *et al.* Celastrol induces unfolded protein response-dependent cell death in head and neck cancer. *Exp Cell Res* 2015, 330: 412–422

12. Hou W, Liu B, Xu H. Celastrol: progresses in structure-modifications, structure-activity relationships, pharmacology and toxicology. *Eur J Medicinal Chem* 2020, 189: 112081

13. Wang SF, Liu KC, Wang XM, He QX, Hou HR. Preliminary study on cardiotoxicity of celastrol to zebrafish embryo. *Chinese Pharmacological Bulletin* 2009, 25: 634–636

14. Wang S, Liu K, Wang X, He Q, Chen X. Toxic effects of celastrol on embryonic development of zebrafish (*Danio rerio*). *Drug Chem Toxicol* 2010, 34: 61–65

15. Sun H, Liu X, Xiong Q, Shikano S, Li M. Chronic inhibition of cardiac Kir2.1 and hERG potassium channels by celastrol with dual effects on both ion conductivity and protein trafficking. *J Biol Chem* 2006, 281: 5877–5884

16. Liu C, Zhang C, Wang W, Yuan F, He T, Chen Y, Wang Q, *et al.* Integrated metabolomics and network toxicology to reveal molecular mechanism of celastrol induced cardiotoxicity. *Toxicol Appl Pharmacol* 2019, 383: 114785

17. Kaufman RJ. Orchestrating the unfolded protein response in health and disease. *J Clin Invest* 2002, 110: 1389–1398

18. Ron D, Walter P. Signal integration in the endoplasmic reticulum unfolded protein response. *Nat Rev Mol Cell Biol* 2007, 8: 519–529

19. Senft D, Ronai ZA. UPR, autophagy, and mitochondria crosstalk underlies the ER stress response. *Trends Biochem Sci* 2015, 40: 141–148

20. Yoshida H. ER stress and diseases. *FEBS J* 2007, 274: 630–658

21. Oyadomari S, Araki E, Mori M. Endoplasmic reticulum stress-mediated apoptosis in pancreatic β-cells. *Apoptosis* 2002, 7: 335–345

22. Minamino T, Kitakaze M. ER stress in cardiovascular disease. *J Mol Cell Cardiol* 2010, 48: 1105–1110

23. Choy KW, Murugan D, Mustafa MR. Natural products targeting ER stress pathway for the treatment of cardiovascular diseases. *Pharmacol Res* 2018, 132: 119–129

24. Wang J, Hu X, Jiang H. ER stress-induced apoptosis: a novel therapeutic target in heart failure. *Int J Cardiol* 2014, 177: 564–565

25. Okada K, Minamino T, Tsukamoto Y, Liao Y, Tsukamoto O, Takashima S, Hirata A, et al. Prolonged endoplasmic reticulum stress in hypertrophic and failing heart after aortic constriction. *Circulation* 2004, 110: 705–712

26. Dally S, Monceau V, Corvazier E, Bredoux R, Raies A, Bobe R, del Monte F, et al. Compartmentalized expression of three novel sarco/endoplasmic reticulum Ca2 + ATPase 3 isoforms including the switch to ER stress, SERCA3f, in non-failing and failing human heart. *Cell Calcium* 2009, 45: 144–154

27. Hamada H, Suzuki M, Yuasa S, Mimura N, Shinozuka N, Takada Y, Suzuki M, et al. Dilated cardiomyopathy caused by aberrant endoplasmic reticulum quality control in mutant KDEL receptor transgenic mice. *Mol Cell Biol* 2004, 24: 8007–8017

28. Fu HY, Mukai M, Awata N, Sakata Y, Hori M, Minamino T. Protein quality control dysfunction in cardiovascular complications induced by anti-cancer drugs. *Cardiovasc Drugs Ther* 2017, 31: 109–117

29. Bagchi AK, Malik A, Akolkar G, Zimmer A, Belló-Klein A, De Angelis K, Jassal DS, et al. Study of ER stress and apoptotic proteins in the heart and tumor exposed to doxorubicin. *Biochim Biophys Acta Mol Cell Res* 2021, 1868: 119039

30. Kerkelä R, Grazette L, Yacobi R, Iliescu C, Patten R, Beahm C, Walters B, et al. Cardiotoxicity of the cancer therapeutic agent imatinib mesylate. *Nat Med* 2006, 12: 908–916

31. Maass AH, Buvoli M. Cardiomyocyte preparation, culture, and gene transfer. *Methods Mol Biol* 2007, 366: 321–330

32. Zinszner H, Kuroda M, Wang X, Batchvarova N, Lightfoot RT, Remotti H, Stevens JL, et al. CHOP is implicated in programmed cell death in response to impaired function of the endoplasmic reticulum. *Genes Dev* 1998, 12: 982–995

33. Yamaguchi H, Wang HG. CHOP is involved in endoplasmic reticulum stress-induced apoptosis by enhancing DR5 expression in human Carcinoma Cells. *J Biol Chem* 2004, 279: 45495–45502

34. Peng X, Pentassuglia L, Sawyer DB. Emerging anticancer therapeutic targets and the cardiovascular system. *Circ Res* 2010, 106: 1022–1034

35. Force T. Introduction to cardiotoxicity review series. *Circ Res* 2010, 106: 19–20

36. Shaker ME, Ashamallah SA, Houssen ME. Celastrol ameliorates murine colitis via modulating oxidative stress, inflammatory cytokines and intestinal homeostasis. *Chem Biol Interact* 2014, 210: 26–33

37. Kim JE, Lee MH, Nam DH, Song HK, Kang YS, Lee JE, Kim HW, et al. Celastrol, an NF-κB inhibitor, improves insulin resistance and attenuates renal injury in db/db mice. *PLoS ONE* 2013, 8: e62068

38. Kannaiyan R, Manu KA, Chen L, Li F, Rajendran P, Subramaniam A, Lam P, et al. Celastrol inhibits tumor cell proliferation and promotes apoptosis through the activation of c-Jun N-terminal kinase and suppression of PI3 K/Akt signaling pathways. *Apoptosis* 2011, 16: 1028–1041

39. Dai Y, Desano J, Tang W, Meng X, Meng Y, Burstein E, Lawrence TS, et al. Natural proteasome inhibitor celastrol suppresses androgen-independent prostate cancer progression by modulating apoptotic proteins and NF-kappaB. *PLoS ONE* 2010, 5: e14153

40. Mou H, Zheng Y, Zhao P, Bao H, Fang W, Xu N. Celastrol induces apoptosis in non-small-cell lung cancer A549 cells through activation of mitochondria- and Fas/FasL-mediated pathways. *Toxicol In Vitro* 2011, 25: 1027–1032

41. Tozawa K, Sagawa M, Kizaki M. Quinone methide tripterine, celastrol, induces apoptosis in human myeloma cells via NF-κB pathway. *Int J Oncol* 2011

42. Yang HS, Kim JY, Lee JH, Lee BW, Park KH, Shim KH, Lee MK, et al. Celastrol isolated from Tripterygium regelii induces apoptosis through both caspase-dependent and -independent pathways in human breast cancer cells. *Food Chem Toxicol* 2011, 49: 527–532

43. Zhou LL, Lin ZX, Fung KP, Cheng CHK, Che CT, Zhao M, Wu SH, et al. Celastrol-induced apoptosis in human HaCaT keratinocytes involves the inhibition of NF-κB activity. *Eur J Pharmacol* 2011, 670: 399–408

44. Kashyap D, Sharma A, Tuli HS, Sak K, Mukherjee T, Bishayee A. Molecular targets of celastrol in cancer: Recent trends and advancements. *Crit Rev Oncol Hematol* 2018, 128: 70–81

45. Yadav P, Jaswal V, Sharma A, Kashyap D, Tuli HS, Garg VK, Das SK, et al. Celastrol as a pentacyclic triterpenoid with chemopreventive properties. *Pharmaceutical Patent Analyst* 2018, 7: 155–167

46. Chadalapaka G, Jutooru I, Safe S. Celastrol decreases specificity proteins (Sp) and fibroblast growth factor receptor-3 (FGFR3) in bladder cancer cells. *Carcinogenesis* 2012, 33: 886–894

47. Liu Z, Ma L, Wen ZS, Hu Z, Wu FQ, Li W, Liu J, et al. Cancerous inhibitor of PP2A is targeted by natural compound celastrol for degradation in non-small-cell lung cancer. *Carcinogenesis* 2014, 35: 905–914

48. Rajendran P, Li F, Shanmugam MK, Kannaiyan R, Goh JN, Wong KF, Wang W, et al. Celastrol Suppresses Growth and Induces Apoptosis of Human Hepatocellular Carcinoma through the Modulation of STAT3/JAK2 Signaling Cascade In Vitro and In Vivo. *Cancer Prevention Res* 2012, 5: 631–643

49. Huang T, Wang Y, Shen Y, Ao H, Guo Y, Han M, Wang X. Preparation of high drug-loading celastrol nanosuspensions and their anti-breast cancer activities in vitro and in vivo. *Sci Rep* 2020, 10: 8851

50. Li HY, Zhang J, Sun LL, Li BH, Gao HL, Xie T, Zhang N, et al. Celastrol induces apoptosis and autophagy via the ROS/JNK signaling pathway in human osteosarcoma cells: an in vitro and in vivo study. *Cell Death Dis* 2015, 6: e1604

51. Sreeramulu S, Gande SL, Göbel M, Schwalbe H. Molecular mechanism of inhibition of the human protein complex Hsp90-Cdc37, a kinome chaperone-cochaperone, by triterpene celastrol. *Angew Chem Int Ed* 2009, 48: 5853–5855

52. Feng L, Zhang D, Fan C, Ma C, Yang W, Meng Y, Wu W, et al. ER stress-mediated apoptosis induced by celastrol in cancer cells and important role of glycogen synthase kinase-3β in the signal network. *Cell Death Dis* 2013, 4: e715

53. Zhong YL, Xu GJ, Huang S, Zhao L, Zeng Y, Xiao XF, An JL, et al. Celastrol induce apoptosis of human multiple myeloma cells involving inhibition of proteasome activity. *Eur J Pharmacol* 2019, 853: 184–192

54. Ren B, Liu H, Gao H, Liu S, Zhang Z, Fribley AM, Callaghan MU, et al. Celastrol induces apoptosis in hepatocellular carcinoma cells via targeting ER-stress/UPR. *Oncotarget* 2017, 8: 93039–93050

55. Bush KT, Goldberg AL, Nigam SK. Proteasome inhibition leads to a heat-shock response, induction of endoplasmic reticulum chaperones, and thermotolerance. *J Biol Chem* 1997, 272: 9086–9092

56. Fribley A, Wang CY. Proteasome inhibitor induces apoptosis through induction of endoplasmic reticulum stress. *Cancer Biol Ther* 2006, 5: 745–748

57. Nawrocki ST, Carew JS, Dunner Jr. K, Boise LH, Chiao PJ, Huang P, Abbruzzese JL, et al. Bortezomib Inhibits PKR-Like endoplasmic reticulum (ER) kinase and induces apoptosis via ER Stress in human pancreatic cancer cells. *Cancer Res* 2005, 65: 11510–11519

58. Fels DR, Ye J, Segan AT, Kridel SJ, Spiotto M, Olson M, Koong AC, et al. Preferential cytotoxicity of bortezomib toward hypoxic tumor cells via

overactivation of endoplasmic reticulum stress pathways. *Cancer Res* 2008, 68: 9323–9330

59. Fu HY, Okada K, Liao Y, Tsukamoto O, Isomura T, Asai M, Sawada T, *et al.* Ablation of C/EBP homologous protein attenuates endoplasmic reticulum–mediated apoptosis and cardiac dysfunction induced by pressure overload. *Circulation* 2010, 122: 361–369

60. Battson ML, Lee DM, Gentile CL. Endoplasmic reticulum stress and the development of endothelial dysfunction. *Am J Physiol Heart Circ Physiol* 2017, 312: H355–H367

61. Tabas I, Ron D. Integrating the mechanisms of apoptosis induced by endoplasmic reticulum stress. *Nat Cell Biol* 2011, 13: 184–190

62. Fu HY, Minamino T, Tsukamoto O, Sawada T, Asai M, Kato H, Asano Y, *et al.* Overexpression of endoplasmic reticulum-resident chaperone attenuates cardiomyocyte death induced by proteasome inhibition. *Cardiovasc Res* 2008, 79: 600–610

63. Timmins JM, Ozcan L, Seimon TA, Li G, Malagelada C, Backs J, Backs T, *et al.* Calcium/calmodulin-dependent protein kinase II links ER stress with Fas and mitochondrial apoptosis pathways. *J Clin Invest* 2009, 119: 2925–2941

64. Scorrano L, Oakes SA, Opferman JT, Cheng EH, Sorcinelli MD, Pozzan T, Korsmeyer SJ. BAX and BAK regulation of endoplasmic reticulum Ca^{2+}: a control point for apoptosis. *Science* 2003, 300: 135–139